applied mechanics

MDPI

Article

Numerical Modeling of Thermomechanics of Antifriction Polymers in Viscoelastic and Elastic-Viscoplastic Formulations

Anastasia P. Bogdanova [1,2], Anna A. Kamenskikh [1,2,*], Andrey R. Muhametshin [1] and Yuriy O. Nosov [1,2]

[1] Laboratory of Digital Engineering of Mechanical Engineering Processes and Production, Perm National Research Polytechnic University, 614990 Perm, Russia; anstasia_pankova@mail.ru (A.P.B.); muhametshin_science@mail.ru (A.R.M.); ura.4132@yandex.ru (Y.O.N.)

[2] Department of Computational Mathematics, Mechanics and Biomechanics, Perm National Research Polytechnic University, 614990 Perm, Russia

* Correspondence: anna_kamenskih@mail.ru; Tel.: +7-(342)-239-15-64

Abstract

The present article relates to the description of phenomenological relations of amorphous material behavior within the framework of viscoelasticity and elastic-viscoplasticity theory, as well as to the creation of its digital analog. Ultra-high-molecular-weight polyethylene (UHMWPE) is considered in the study. The model is based on the results of a series of experimental studies. Free compression of cylindrical specimens in a wide range of temperatures [−40; +80] °C and strain rates [0.1; 4] mm/min was performed. Cylindrical specimens were also used to determine the thermal expansion coefficient of the material. Dynamic mechanical analysis (DMA) was performed on rectangular specimens using a three-point bending configuration. Maxwell and Anand models were used to describe the material behavior. In the framework of the study, the temperature dependence of a number of parameters was established. This influenced the mathematical formulation of the Anand model, which was adapted by introducing the temperature dependence of the activation energy, the initial deformation resistance, and the strain rate sensitivity coefficient. Testing of the material models was carried out in the process of analyzing the deformation of a spherical bridge bearing with a multi-cycle periodic load. The load corresponded to the movement of a train on a bridge structure, without taking into account vibrations. It is shown that the viscoelastic model does not describe the behavior of the material accurately enough for a quantitative analysis of the stress–strain state of the structure. It is necessary to move on to more complex models of material behavior to minimize the discrepancy between the digital analog and the real structure; it has been established that taking into account plastic deformation while describing UHMWPE would allow this to be performed.

Keywords: amorphous material; UHMWPE; viscoelasticity; elastic-viscoplasticity; spherical bridge bearing; polymer sliding layer; plastic deformation

Check for updates

Received: 8 November 2025
Revised: 9 December 2025
Accepted: 20 December 2025
Published: 24 December 2025

Copyright: © 2025 by the authors. Licensee MDPI, Basel, Switzerland. This article is an open access article distributed under the terms and conditions of the Creative Commons Attribution (CC BY) license.

1. Introduction

1.1. Target of Research

The purpose of the present work is to create a viscoelastic and elastic-viscoplastic behavior model of low-friction polymer materials and to perform their comparative analysis. This study employs an experimental methodology for investigating such materials, implemented here using ultra-high-molecular-weight polyethylene (UHMWPE) as an example. The article also provides a description of phenomenological relations for the stress–strain

state of the material within the framework of viscoelasticity and elastic-viscoplasticity over a wide range of operating temperatures. Testing of the material behavior models was carried out using the example of multi-cycle deformation of a spherical bridge bearing with an antifriction UHMWPE layer.

The objectives of the study include:

1. Performing a series of experimental studies of deformation behavior of UHMWPE specimens, specifically: dynamic mechanical analysis (DMA); measuring the thermal expansion coefficient (CTE)free compression of cylindrical specimens.
2. The determination of phenomenological relationships to describe material behavior in modern computer-aided design (CAD) systems, taking into account experimental data.
3. The formation of vectors of unknown parameters of viscoelastic and elastic-viscoplastic models for further identification. The creation of numerical analogs of experiments for verification of model identification results and the identification of phenomenological relation parameters based on experimental data.
4. The approbation of the digital analog of the material in the context of the problem of multi-cycle deformation of a spherical bridge bearing with a sliding layer made of UHMWPE.
5. An analysis of the influence of UHMWPE mathematical models on the stress–strain state of the antifriction layer of a spherical bridge bearing.

Complex phenomenological models will help to minimize the discrepancy between the real structure and its numerical analog. Experimental studies in a wide temperature range will make it possible to evaluate the thermomechanics of the antifriction material.

1.2. Problem Context and Description

Polymers with antifriction properties are widely used in many fields of human activity [1–4]. Materials of this type are used as coatings and interlayers to minimize wear of the interface surfaces of the elements. A distinctive feature of antifriction materials is their friction coefficients, which are less than 0.2. They may also be significantly lower than 0.2 and be only 0.01 or less under various operating conditions [5,6]. Such materials are used as relatively thin protective, protective-strengthening, antifriction coatings, and interlayers in various fields of science and technology. Antifriction materials in friction units can increase the durability and reliability of the structure, its service life, and overhaul periods.

Active development in the polymer industry makes it possible to replace conventional materials with polymers [7–9], which leads to the positive effects: weight reduction, increased wear resistance, improved friction properties, etc. Thus, the authors of [9] describe the revolutionary developments of the polymer industry in the field of increasing the strength and reducing the weight of the material. The role of polymers in future innovations is also emphasized. However, the introduction of new materials often entails changes in the technological process, system geometry, and technical documentation [10,11]. This, in turn, raises the question of mathematically describing the behavior of the materials in conditions close to operational conditions for creating digital analogs [12]. However, formulation of the numerical analogs of the materials requires a large amount of experimental data and the implementation of a rather complex mathematical apparatus [13–15].

Polytetrafluoroethylene (PTFE) is widely used among the antifriction materials [16–18]. The material has the best antifriction properties compared to analogs under high loads, heat resistance, etc. However, it has limitations in use due to its high wear rate and low yield strength. This is particularly evident in the systems operating under multi-cycle loading [19,20]. Nowadays, PTFE is being replaced with new materials. UHMWPE is one

of the possible alternatives to PTFE [21–23]. It demonstrates better physical and mechanical properties [24–26] and also has a wider operating temperature range.

The lack of information on the properties of antifriction polymers and composites is still noted [27–29]. It is largely due to the constant improvement of the material formulations, as well as the emergence of new manufacturers and new materials [30]. This significantly reduces the prospects of using new materials in the industry. Quite a large number of experimental studies are required to evaluate the behavior of the materials and formulate their numerical analogs. The main types of experimental studies are: DMA [31,32]; thermomechanical analysis [15,33]; constrained/free compression [34]; tribological testing [35,36]; chemical analysis [37,38], etc. An experimental study allows for an initial assessment of the possibility of using the material in certain technological processes and operating conditions. However, for a quality-assuring approach, a synergy is used between the experimental study and the formulation of a numerical analog of the material (of a structure, a system) [39,40].

Mathematical models qualitatively and quantitatively characterizing the behavior of materials are necessary to formulate a numerical analog of structures and systems with minimal differences from reality. The list of mathematical models that can be used to characterize polymers and composites is quite long. These are models describing materials within the framework of elastoplasticity theory [28,41], viscoelasticity theory [28,42], and elastic-viscoplasticity theory [43,44]. Elastoplastic models can describe the behavior of a material both qualitatively and quantitatively. However, they are limited to static problems [28]. Models of viscoelasticity and elastic-viscoplasticity theory should be used to predict material performance, taking into account the time factor. However, using complex models increases the cost of computing resources. To minimize the cost of computing resources, a preliminary evaluation of the models' performance can be carried out in planar and axisymmetric formulations. Two behavior models of the antifriction material were considered in the current study: the viscoelastic model (Maxwell body) and the elastic-viscoplastic model (Anand model).

Analysis of the deformation behavior of an L-100 spherical bridge bearing with a polymer sliding layer was considered for testing the UHMWPE behavior models [27]. A bridge bearing is an important structural element. A bridge bearing determines the maintenance-free service life of bridgework as a whole [45–47]. Mathematical simulation of the antifriction layer material behavior makes it possible to evaluate the operation of the structure in regular and emergency situations [27,45]. Replacement of the antifriction layer material can also be considered using digital analogs of the material and design [9].

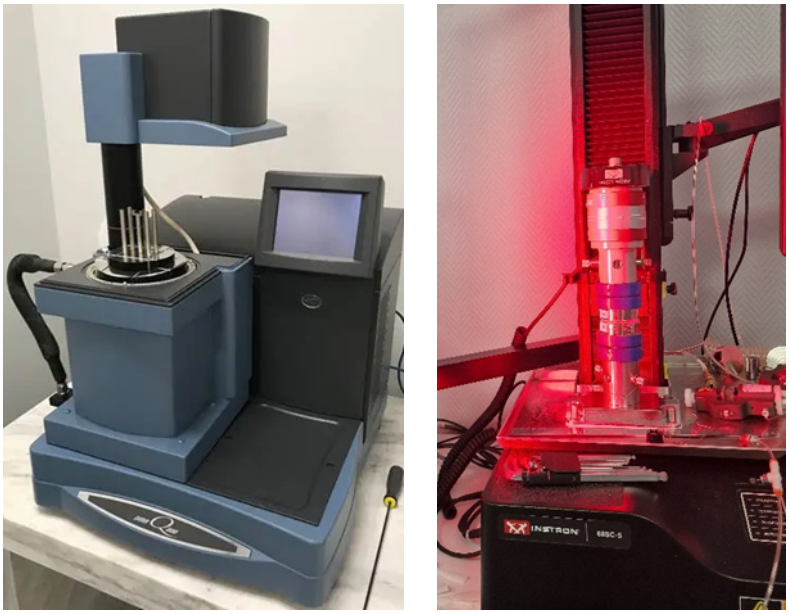
An experimental research method providing a possibility of automatically identifying the parameters of mathematical models was developed. Viscoelastic and elastic-viscoplastic material behavior models are based on experimental data. A digital analog of a spherical bridge bearing, taking into account the multi-cycle loading, was formulated to test the models. A multivariate analysis of the antifriction layer material behavior, for various mathematical models describing its behavior, was carried out.

2. Materials and Methods

2.1. Experimental Study

A series of experimental studies needed to be carried out to determine the mathematical model of the material. Two main types of experiments were selected: DMA and CTE determination using DMA Q800 (TA Instruments, New Castle, DE, USA) (Figure 1a); and uniaxial stress state (USS) testing using Instron 68SC-5 (Instron® Corporation, Norwood, MA, USA) (Figure 1b). A thermal field at sub-zero temperatures was created using liquid nitrogen as part of the experiments on a DMA Q800 unit. A 24 h exposure at a preset tem-

perature in an ST-64-70H temperature chamber (SONACME Technology Co., Dongguan City, China) was used to record the temperature during the USS experiment. An AVE2 video extensometer (Instron® Corporation, Norwood, MA, USA) was used to record the results of the uniaxial compression testing.



(**a**) (**b**)

Figure 1. Experimental setups: (**a**) is DMA Q800; (**b**) is Instron 65SC-5.

Cylindrical specimens 4 mm × 4 mm were used in the experiments for uniaxial compression and CTE determination. Rectangular specimens with average dimensions of 60 mm × 12 mm × 3 mm were used in DMA tests. A temperature range of −40 °C to +80 °C was considered. To ensure the static significance of the results, at least 3 tests were conducted for each type of thermal strength loading. Experimental studies were conducted on UHMWPE specimens (AlfaTech LLC, Perm, Russia). The specimens for experimental testing are shown in Figure 2.

Brief experimental procedure:

1. **DMA:** Testing of the specimens was carried out according to the three-point bending principle. The specimens were fixed with two clamps equipped with roller bearing supports. This eliminated the clamping effect when the specimen was deformed. Gradual heating of the specimen to +80 °C took place in the measuring unit chamber during the 1st stage of the experiment. The heating time was 20 min. After reaching the required temperature, the specimen was kept at +80 °C for 10 min. An oscillating load was applied to the center of the specimen in the 2nd stage of the experiment. The frequency of exposure was 1 Hz. Gradual cooling to −40 °C was carried out in increments of 2 °C/min.
2. **TEC:** Testing of the specimens was carried out according to the free compression principle. Cylindrical specimens were placed in compression clamps. To minimize compressive strain, a load of 0.005 N was applied to the specimen. The load did not exceed 0.001% at a temperature of +80 °C, allowing the specimen to be further subjected to thermal deformation. For the material under consideration, CTE in the studied temperature range was assumed to be constant. This is due to the fact that the glass transition temperature did not fall within the temperature range from −40 °C to +80 °C (according to DMA results). In the first stage, the specimen was cooled from room temperature to −40 °C. In the second and third steps of the exper-

iment, the specimen was gradually heated to +20 °C and +80 °C, correspondingly, while recording the temperature deformations of the specimen.

3. **USS:** Testing of the specimens was carried out according to the free compression principle. Before testing, the specimens were kept for 24 h at the preset temperature in a specialized thermal chamber. Additional elements and media were used for forming the interface of the specimens with the press plates to minimize friction and barrel distortion: TsIATIM-221F grease (Ftorpolimernye Tehnologii, Tomsk, Russia) and Teflon film (Yangzhong Dongxu Polymer Material Co., Ltd., Yangzhong, China). The scheme of connecting the specimen with the experimental unit plates is as follows: grease, Teflon film, grease, then specimen. This treatment pattern was used on all mating surfaces. The following four strain rates were considered: 0.1 mm/min (2.5%/min), 1 mm/min (25%/min), 2 mm/min (50%/min), and 4 mm/min (100%/min).

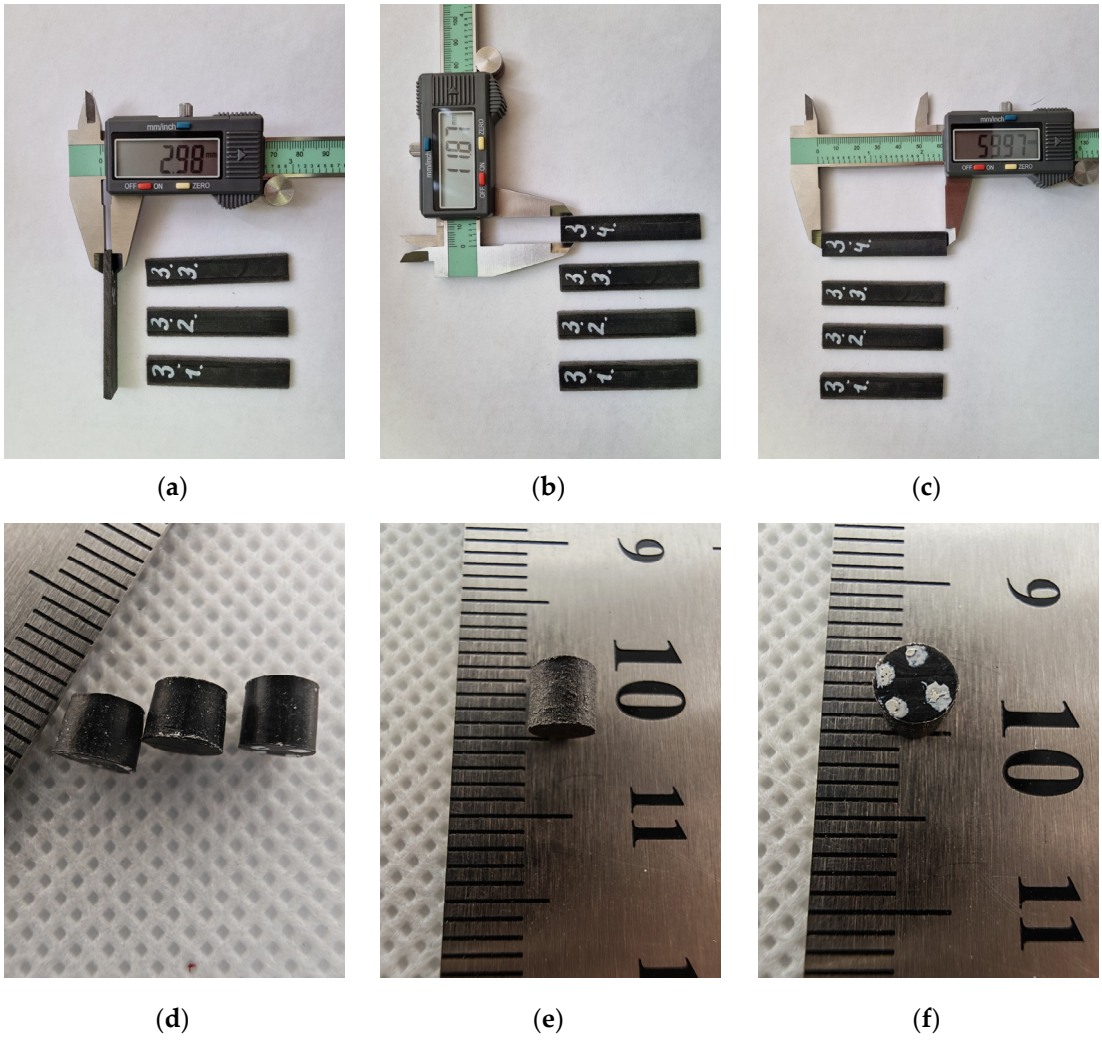


Figure 2. Samples: (**a**–**c**) are rectangular for DMA; (**d**–**f**) are cylindrical for USS and TEC.

DMA makes it possible to obtain data without leaving the linear viscoelasticity zone. This provided a means for characterizing the material using simple models, such as a generalized Maxwell body [48,49]. In the experiment, the specimen was subjected to periodic action with a frequency of 1 Hz with a temperature change of 2 °C/min. The time dependence of stress (1) and strain (2) was as follows:

$$\sigma(t) = \sigma_0 \sin(\omega t + \varphi), \quad (1)$$

$$\varepsilon(t) = \varepsilon_0 \sin(\omega t). \quad (2)$$

where σ_0 is maximum specimen stress; ε_0 is maximum specimen strain; φ is lag angle. The last parameter characterizes the phase shift in stress and strain. A graphic illustration of the phase shift is shown in Figure 3.

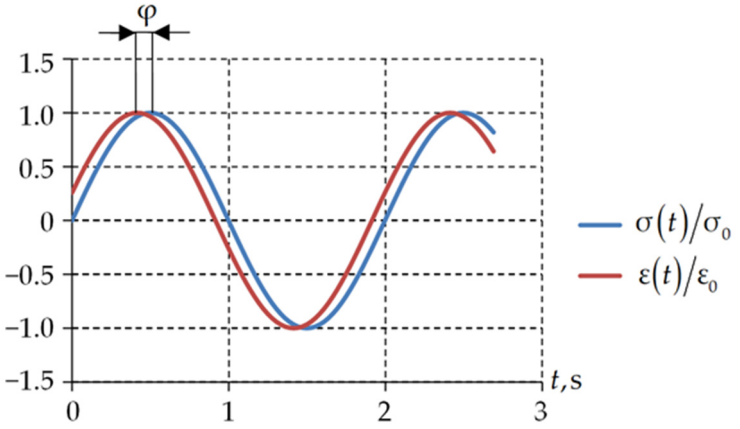


Figure 3. Phase shift angle.

The phase shift angle is a parameter for evaluating the viscoelasticity of the material. A body has viscoelasticity properties if the phase shift angle is in the range $(0; \pi/2)$. This parameter makes it possible to go to the Young modulus components:

$$E' = \sigma_0/\varepsilon_0 \cos(\varphi), \quad (3)$$

$$E'' = \sigma_0/\varepsilon_0 \sin(\varphi), \quad (4)$$

where E' is a storage modulus, and E'' is a loss modulus. The storage modulus shows the effect of the elastic part on the deformation behavior of the specimen, and the loss modulus shows the effect of its viscous part.

The complex elastic modulus is determined by Formula (5) via E' and E'':

$$E^* = \sqrt{(E')^2 + (E'')^2}. \quad (5)$$

Studying the material only within the linear theory was the main limitation. It can result in large discrepancies with respect to the actual behavior of the material, since plasticity is observed in materials of this class [50]. Taking into account the plastic deformation of the material plays an important role in obtaining a high-quality digital analog.

A series of USS experiments at various temperatures and strain rates were conducted to determine the level of plastic deformations. During the experiments, the actual displacement values were recorded. The forces were determined on the crosshead, and for the transition to stress and strain, the following relationships were used:

$$\sigma = F/S, \quad (6)$$

$$\varepsilon = \Delta h/h_0, \quad (7)$$

where F is a force on the crosshead; S is a contact surface area; Δh is the specimen height change; and h_0 is the initial specimen height.

2.2. Mathematical Models of Material Behavior

The specification of mathematical models of a materials' behavior is an important trend in computer engineering development. A high-quality specification of a materials' behavior makes it possible to predict the behavior of the structure with greater accuracy. Identification of the empirical parameters of mathematical models is based on the author's

algorithm [32]. To do this, it is necessary to form a vector of unknowns for each of the considered material behavior models.

2.2.1. Viscoelastic Model

The viscoelastic model was widely used to describe the behavior of amorphous materials [51,52]. A Maxwell body is one of the most common models [53]. The model makes it possible to describe the time dependence of the complex elastic modulus. The general form of the defining relation is:

$$\boldsymbol{\sigma} = \int_0^t 2G(t-\tau)\dot{\mathbf{e}}(\tau)d\tau + \mathbf{I}\int_0^t K(t-\tau)\dot{\theta}(\tau)d\tau, \quad (8)$$

where $\boldsymbol{\sigma}$ is the Cauchy stress tensor; $\dot{\mathbf{e}}$ is strain deviator; $\dot{\theta}$ is volumetric deformation; $\mathbf{I}$ is unit vector; $G(t)$, and $K(t)$ are shear modulus and bulk compression modulus, correspondingly.

Due to the condition of the constancy of the bulk compression modulus, relation (8) takes the form (9):

$$\boldsymbol{\sigma} = \int_0^t 2G(t-\tau)\dot{\mathbf{e}}(\tau)d\tau + \mathbf{I}K\theta. \quad (9)$$

Prony series are used to describe the dependence of the shear modulus on time:

$$G(t) = G_0\left(\alpha_\infty + \sum_{i=1}^{N_p}\left(\alpha_i e^{-t/\tau_i}\right)\right), \quad (10)$$

where G_0 is the initial value of the shear modulus at t = 0; α_i is relative shear modulus; N_p is the number of members of a series; τ_i is relaxation times. From the conditions $G_0 = G|_{t=0}$, $G_\infty = G|_{t=\infty}$ it follows that $\alpha_i = G_\infty/G_0$, $\sum_{i=1}^{N_p}\alpha_i = (G_0 - G_\infty)/G_0$. The reference time is used to describe the temperature effect:

$$\tau'_i = \tau_i / A_{WLF}(T), \quad (11)$$

where $A_{WLF}(T) = C_1(T - T_r)/[C_2 + (T - T_r)]$ is Williams-Landel-Ferry (WLF) temperature-time similitude; C_1, and C_2 are empirical constants; T is temperature at a current moment of time; T_r is glass transition temperature. Taking into account the WLF temperature-time similitude, relation (10) takes the form:

$$G(t) = G_0\left(\alpha_\infty + \sum_{i=1}^{N_p}\left(\alpha_i e^{-t/\tau'_i}\right)\right). \quad (12)$$

For the transition to the elastic modulus, we use relation (10):

$$E(t) = E_0\left(\beta_\infty + \sum_{i=1}^{N_p}\left(\beta_i e^{-t/\tau_i}\right)\right), \quad (13)$$

where E_0 is the initial value of the shear modulus at t = 0; β_i is the relative elasticity modulus.

Let us assume that the relaxation times for shear and tension/compression coincide. Then the relation for the relative elastic modules can be represented as:

$$\sum_{i=1}^{N_p}\alpha_i = \sum_{i=1}^{N_p}\beta_i \cdot D, \quad (14)$$

where $D = [(G_0 - G_\infty)E_0]/[(E_0 - E_\infty)G_0]$. The dependence of the initial and final shear modulus on elastic modulus has forms $G_0 = E_0/(2 + 2\nu_0)$, $G_\infty = E_\infty/(2 + 2\nu_\infty)$. The Poisson ratio at the final time moment can be found from the relation $K_\infty = K^* = E_\infty/(3 - 6\nu_\infty)$. This is due to the constancy of the bulk compression modulus $K^* = E_0/(3 - 6\nu_0) = \text{const}$. The formula for determining the Poisson ratio at the final time moment is

$$\nu_\infty = 0.5 - E_\infty/(6K^*). \quad (15)$$

The parameters of the Maxwell body viscoelastic model described with the Prony series can be found from the tension/compression experimental data. The defining relation in the case of uniaxial tension/compression takes the form (16):

$$\sigma(t) = \int_0^t \left[E_\infty + E_0 \sum_{i=1}^{N_p} \left(\beta_i e^{-(t-\psi)/\tau_i'}\right)\right] d\varepsilon(\psi). \quad (16)$$

Taking into account Formula (2), relation (16) can be transformed to the form (17):

$$\sigma(t) = \varepsilon_0 \left\{ \sin(\omega t) \left[E_\infty + \omega^2 E_0 \sum_{i=1}^{N_p} \tau_i'^2 \beta_i / \left(1 + \tau_i'^2 \omega^2\right)\right] + \cos(\omega t) \omega E_0 \sum_{i=1}^{N_p} \tau_i' \beta_i / \left(1 + \tau_i'^2 \omega^2\right) \right\}. \quad (17)$$

Similarly to (3) and (4), the storage modulus (18) and loss modulus (19) will have the form

$$E' = E_\infty + \omega^2 E_0 \sum_{i=1}^{N_p} \tau_i'^2 \beta_i / \left(1 + \tau_i'^2 \omega^2\right), \quad (18)$$

$$E'' = \omega E_0 \sum_{i=1}^{N_p} \tau_i' \beta_i / \left(1 + \tau_i'^2 \omega^2\right). \quad (19)$$

The storage modulus and loss modulus are determined experimentally.

The vector of unknowns for the model being considered will have the form:

$$\mathbf{x} = \left\{\beta_i,\ i = \overline{1, N_p};\ C_1; C_2; T_r\right\}. \quad (20)$$

2.2.2. Elastic-Viscoplastic Model

The Anand model was actively used for describing the elastic-viscoplastic behavior of various materials [54–56]. The Anand model has recently been considered to describe the behavior of polymeric materials [55,57]. The possibility of a more accurate description of the material appears due to the consideration of activation energy, the strain rate parameter, and other empirical parameters of the model. The defining relation of the elastic-viscoplastic behavior has the form:

$$\dot{\hat{\varepsilon}}^v(t) = \dot{\varepsilon}_{Eqv}^v(t)\left(3/2\ \hat{s}/\sigma_{Eqv}\right), \quad (21)$$

where $\dot{\hat{\varepsilon}}^v$ is the tensor of viscoplastic strain rate; $\dot{\varepsilon}_{Eqv}^v = \sqrt{2/3\left(\dot{\hat{\varepsilon}}^v : \dot{\hat{\varepsilon}}^v\right)}$ is equivalent viscoplastic strain rate; $\hat{s} = \hat{\sigma}(t) - \sigma(t)\hat{E}$ is stress deviator; $\sigma(t) = \sum_{i=1}^{3} \sigma_{ii}(t)/3$ is mean stress; $\sigma_{Eqv} = \sqrt{3/2(\hat{s} : \hat{s})}$ is equivalent stress. The equivalent viscoplastic strain rate is formulated with a number of empirical parameters:

$$\dot{\varepsilon}_{Eqv}^v = A e^{-U/RT} \left[\sinh\left(\xi \sigma_{Eqv}/s\right)\right]^{1/m}, \quad (22)$$

where $Ae^{-U/(RT)} = k$ is the Arrhenius equation, defining viscosity by the expression $\eta = 1/k$; A is pre-exponential factor $[1/(\mathrm{Pa} \cdot \mathrm{s})]$; U is activation energy [J/mole]; R is universal gas constant $[\mathrm{J}/(\mathrm{mole} \cdot \mathrm{K})]$; T is absolute temperature [K]; s is yield strength initial value [MPa]; dimensionless constant m is strain rate sensitivity factor; dimensionless constant ξ, is empirical constant.

The evolutionary equation for yield strength has the form (23):

$$\dot{s} = \left\{h_0 (|B|)^a B/|B|\right\}, \quad (23)$$

$$B = 1 - s/s^* \quad (24)$$

$$s^* = \widehat{s}\left[\dot{\varepsilon}_{Eqv}^v / A e^{U/RT}\right]^n, \quad (25)$$

where h_0 is the hardening/softening parameter [MPa]; dimensionless constant a is the strain rate sensitivity factor for hardening/softening; $\widehat{s}$ is yield strength saturation parameter [MPa]; dimensionless constant n is rate to yield strength change sensitivity parameter.

The vector of unknowns for the elastic-viscoplastic model has the form:

$$\mathbf{x} = \left\{ s_0;\ U;\ A;\ \xi;\ m;\ h_0;\ \widehat{s};\ n;\ a \right\}. \tag{26}$$

The standard Anand model has limitations when describing amorphous materials [58]. To improve the quality of the material behavior description, the dependence of a number of parameters on temperature will be introduced into the model [59,60]: of activation energy (27), of yield strength (28), and of the strain rate sensitivity factor (29).

$$U(T) = U_1\left(1 + U_2 e^{U_3/(T+273.15)}\right)\left(1 + U_4 e^{U_5/(T+273.15)}\right), \tag{27}$$

$$s_0(T) = s_{01}\left(1 + s_{02} e^{s_{03}/(T+273.15)}\right)\left(1 + s_{04} e^{s_{05}/(T+273.15)}\right), \tag{28}$$

$$m(T) = m_1\left(1 + m_2 e^{m_3/(T+273.15)}\right)\left(1 + m_4 e^{m_5/(T+273.15)}\right), \tag{29}$$

where U_i, s_{0i}, m_i are the empirical parameters of relations (27)–(29).

Dependencies (27)–(29) were introduced based on the data presented in the article by Sanditov et al. [61].

The resulting vector of unknowns of the elastic-viscoplastic model takes the form:

$$\mathbf{x} = \left\{ U_i;\ s_{0i};\ m_i;\ A;\ \xi;\ h_0;\ \widehat{s};\ n;\ a \right\},\ i = \overline{1:5}. \tag{30}$$

2.3. Spherical Bridge Bearing Model

Deformation behavior analysis of a spherical bridge bearing L-100 (AlfaTech LLC, Perm, Russia) was performed for various behavior models of the UHMWPE antifriction layer. The problem is considered in an axially symmetric formulation and includes a contact assembly comprising a top steel plate with a polished spherical segment (1), a bottom steel plate with a spherical cutout (2) for the antifriction layer (3) (Figure 4). The model does not take into account cavities for lubricant in the antifriction layer (3). The axially symmetric model of the structure allows testing material behavior models of the antifriction layer under different loading conditions without any significant computational power costs.

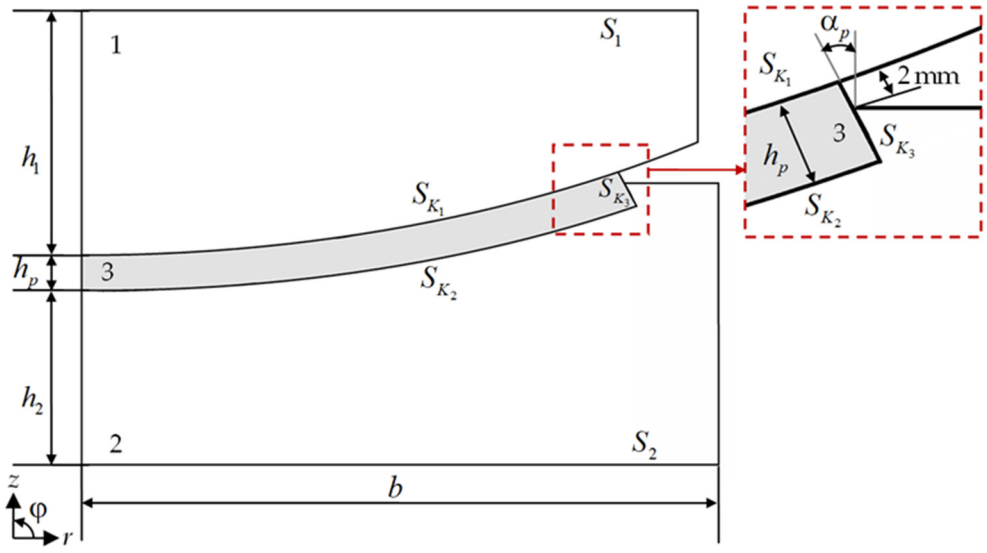


Figure 4. Computational scheme of the spherical bridge bearing: 1 and 2 are top and bottom steel plates, correspondingly; 3 is polymer sliding layer; red square is enlarged image of the interlayer edge.

The overall dimensions of L-100: total height 54 mm $(h = h_1 + h_p + h_2 = 20 + 4 + 30)$, width and depth 155 mm $(B = 2b)$; the height of the layer edge not contacting with the

bottom steel plate (the antifriction layer protrusion) is approximately 2 mm, the antifriction layer slope angle is $\alpha_p = 30°$. The structure is designed for a maximum vertical load of 1000 kN (~55 MPa pressure on the upper spherical balancer).

At the interfaces of the antifriction layer with steel elements of the structure $S_{K_1} - S_{K_3}$, a friction contact is implemented with an unknown in advance distribution pattern of the contact state zones (sticking, slipping, non-contact) [62]:

- sliding

$$u_n^1 \neq u_n^2,\ u_\tau^1 \neq u_\tau^2,\ \sigma_n^1 = \sigma_n^2,\ \sigma_{n\tau}^1 = \sigma_{n\tau}^2,$$

when $|\sigma_{n\tau}| = \mu(\sigma_n)|\sigma_n|$;

- non-contact

$$\left|u_n^1 - u_n^2\right| \geq 0,\ \sigma_{n\tau} = \sigma_n = 0;$$

- full attachment (adhesion)

$$\vec{u}^1 = \vec{u}^2,\ \sigma_n^1 = \sigma_n^2,\ \sigma_{n\tau}^1 = \sigma_{n\tau}^2,$$

where $\mu(\sigma_n)$ is the coefficient of friction, τ is the designation of the axis that lies in the plane tangent to the contact surface, u_n is displacement along the normal to the corresponding contact boundary, u_τ is displacement in the tangent plane, σ_n is stress along the normal to the contact boundary, $\sigma_{n\tau}$ are tangential stresses at the contact boundary, and 1–2 are conditional numbers of interface surfaces that belong to different bodies. The steel-polymer friction coefficient was selected according to the manufacturer's regulatory documents of the supporting parts and is equal to 0.04 (maximum coefficient value).

The problem was implemented using the finite element method in ANSYS Mechanical APDL 2021R2 (Livermore, CA, USA). The general mathematical formulation of the problem and the analysis of the system digitalization degree effect on the numerical solution were previously described in [63]. Eight elements across the interlayer thickness could be sufficient to solve the problem in an elastic-plastic setup. A finite element mesh with 16 elements across the interlayer thickness was used to obtain a higher-quality solution. The convergence of the numerical solution was tested using a viscoelastic model of UHMWPE (Figure 5). It was confirmed that 8–16 elements across the interlayer thickness are sufficient to obtain a high-quality solution. Convergence was investigated at the bearing nominal load.

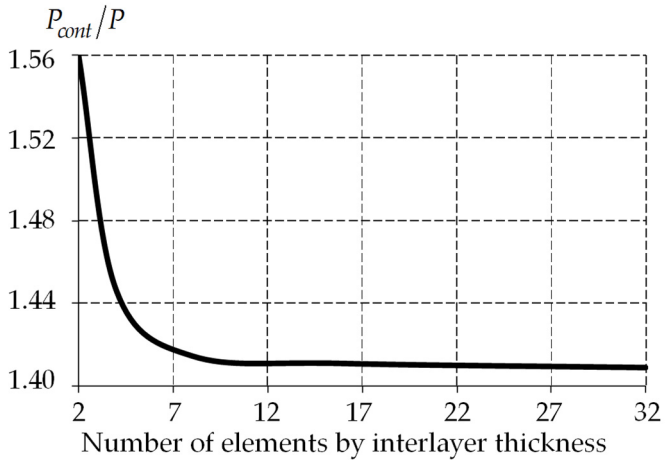


Figure 5. Convergence of the numerical solution.

The finite element discretization of the spherical bearing model is shown in Figure 6.

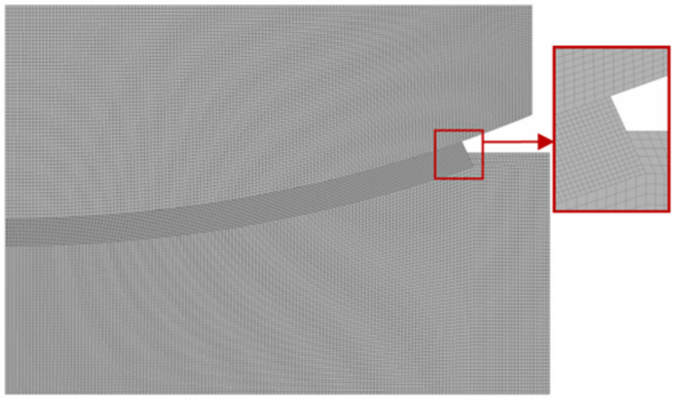


Figure 6. Finite element mesh: red square is enlarged image of the interlayer edge.

PLANE182 axisymmetric quadrilateral elements with Lagrangian approximation. Surface-to-surface contact interaction was modeled using the contact element pair CONTA171 and TARGE169. The primary procedures for constructing finite element analogs were based on the Galerkin method, with basic functions selected to have compact support, as per the finite element method. A step-by-step loading algorithm was used, with iterative refinement of the distribution of contact zones, penetration values, and contact forces. The iterative procedure continued until the results of two consecutive iterations produced contact force and penetration values within the specified accuracy.

Cyclic loading of the bridge bearing was considered to analyze the operation of the material model considered in the context of viscoelasticity and elastic-viscoplasticity theory. The loading cycle is shown in Figure 7.

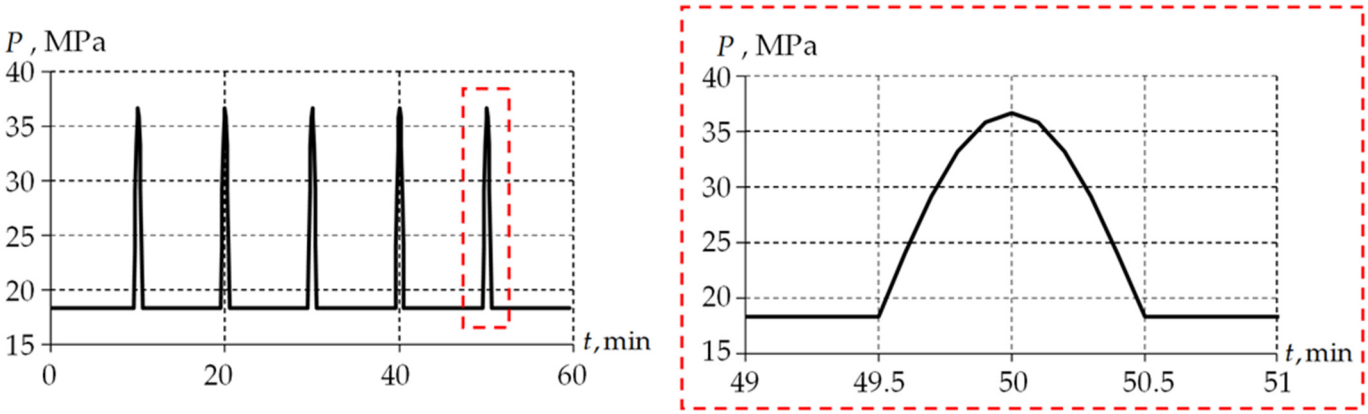


Figure 7. Loading diagram of a spherical bridge bearing: on the right, a red rectangular area is shown enlarged, demonstrating one loading cycle.

A sinusoidal increase in the load level takes place once in a 10 min loading cycle: the minimum level corresponds to the absence of load from transport on the bridge bearing; a sinusoidal increase in the load corresponds to transport passing along the bridge bearing. The model makes it possible to estimate the stress–strain state of the structure in a first approximation for various behavior models of the antifriction layer under multi-cycle loading conditions.

3. Results

3.1. Experimental Studies

3.1.1. Dynamic Mechanical Analysis

The characteristics of the storage modulus E', loss modulus E'', and the loss angle tangent, defined with the formula $\tan\delta = E'/E''$, were obtained in a series of tests. The average characteristics are presented in Figure 8.

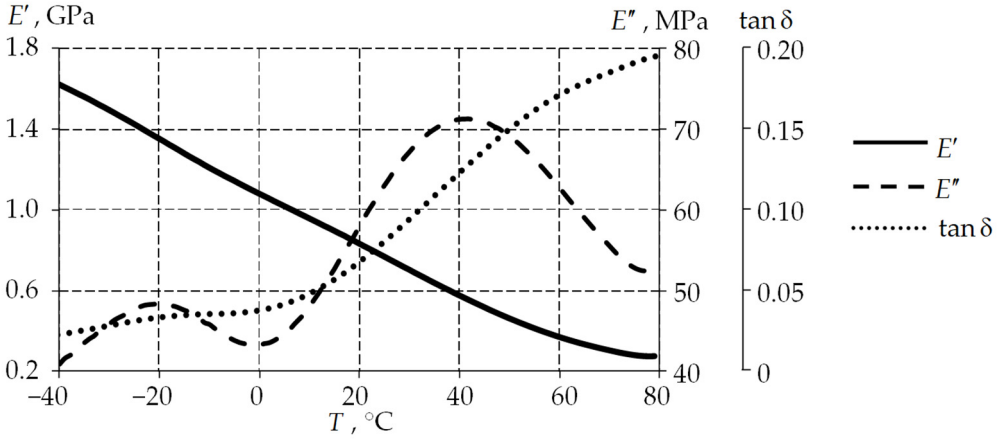


Figure 8. Temperature dependences of the storage modulus, loss modulus, and the loss angle tangent of UHMWPE.

The storage modulus decreases as the temperature increases. As the elastic modulus decreases, the material becomes more plastic. The conclusion that the glass transition/softening temperature of the UHMWPE material does not fall within the range under consideration can be made by analyzing the change in the loss modulus and the loss angle tangent.

3.1.2. Free Compression of the Cylindrical Specimens

In the series of conducted experiments, all tested specimens were subjected to 10% deformation from their original height at various strain rates and temperatures. The specimens before and after straining are shown in Figure 9.



(**a**) (**b**) (**c**)

Figure 9. Cylindrical specimens: (**a**) is before straining; (**b**,**c**) are after straining at different angles.

The difference between the experimental data in the temperature range is on average about 2–5% at a low strain rate of 0.1 mm/min. It decreases with increasing strain rate and is less than 1%. The arithmetic mean value of the experimental data for all strain rates was obtained at various temperatures. Displacement-force dependencies were recalculated to stress–strain dependencies. The free compression modulus and the Poisson ratio were obtained based on relations of Section 2 for the temperature range [−40; +80] °C.

The free compression modulus and the Poisson ratio were approximated using relations (31) and (32), correspondingly:

$$E = E_1\left(E_2 + e^{E_3/(T+273.15)}\right)\left(E_4 + e^{E_5/(T+273.15)}\right), \quad (31)$$

$$\nu = \nu_1\left(\nu_2 + e^{\nu_3/(T+273.15)}\right)\left(\nu_4 + e^{\nu_5/(T+273.15)}\right), \quad (32)$$

where $E_1 - E_5$, $\nu_1 - \nu_5$ are empirical constants (see Tables 1 and 2, correspondingly).

Table 1. Empirical constants for description E.

Empirical Constants	E_1, MPa	E_2	E_3, K	E_4	E_5, K
Value	2.121×10^{-5}	6.388×10^{-3}	2048	6.014×10^{8}	−1355

Table 2. Empirical constants for description ν.

Empirical Constants	ν_1	ν_2	ν_3, K	ν_4	ν_5, K
Value	0.00016	−0.95978	5.912088	61,666.38	229.2025

The obtained results are presented in Figure 10.

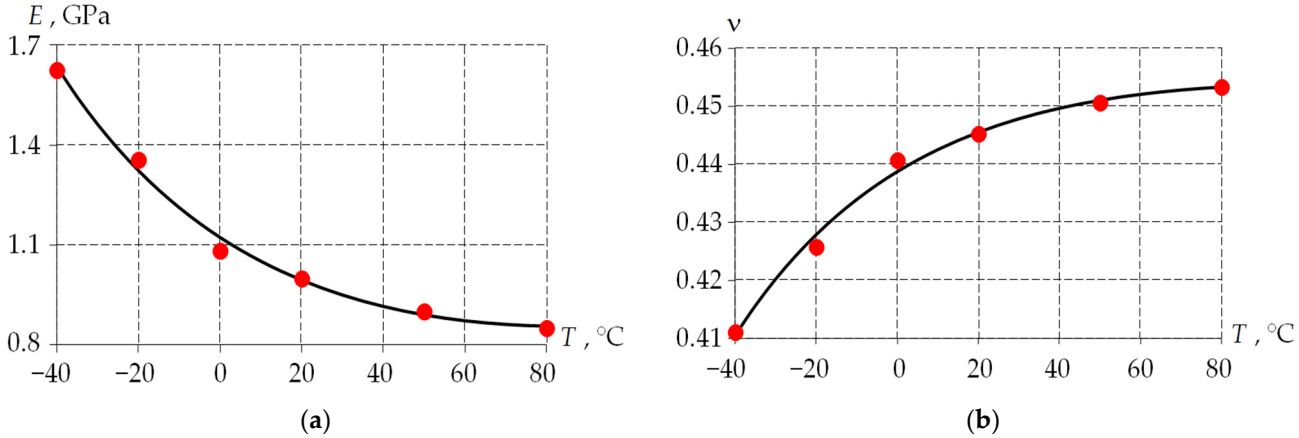


Figure 10. The elastic modulus (**a**) and the Poisson ratio (**b**) dependencies on temperature, obtained in the series of USS tests: dots is averaged data; solid line is approximation.

The elastic compression modulus decreases with increasing temperature, and the Poisson ratio increases.

3.1.3. Thermal Expansion Coefficient

UHMWPE under consideration has a stable structure in the temperature range [−40; +80] °C (determined by DMA), and therefore, CTE was measured at two control points: −40 °C and +80 °C. The discrepancy between the measurement results is less than 1%. The average value $\alpha = 1.81328 \times 10^{-5}$.

3.2. Identification of Mathematical Models

Based on experimental data, material behavior model parameters were obtained. Identification was performed as part of a parameterized optimization algorithm. The algorithm included the possibility of choosing: (a) the simulation model of experiments (three-point bending, free compression); and (b) the material behavior model. The iterative procedure of searching parameters of the vector of unknowns was stopped when the difference between experimental data and the simulation model became less than 5%.

3.2.1. Maxwell Model Based on the Prony Series

A single vector of unknown parameters is determined for the entire temperature range. The 40 $\alpha_i - \beta_i$ pairs were obtained and are presented in Table 3. A model parameters number were also found for its numerical implementation: $C_1 = 288.38$, $C_1 = 1393.95$,

$T_r = 274.12$ K, $E_0 = 1624.77$ MPa, and $E_\infty = 280.55$ MPa. The parameters were found by solving the inverse problem and are not unique. The model can be refined, for example, after experimentally determining the glass transition temperature.

Table 3. The 40 $\alpha_i - \beta_i$ paris.

i	α_i	β_i	i	α_i	β_i	i	α_i	β_i	i	α_i	β_i
1	3.08×10^{-2}	1.00×10^{-9}	11	3.75×10^{-2}	2.73×10^{-2}	21	6.33×10^{-2}	7.44×10^{5}	31	2.79×10^{-3}	2.03×10^{13}
2	3.14×10^{-2}	5.54×10^{-9}	12	2.53×10^{-2}	1.51×10^{-1}	22	6.45×10^{-6}	4.12×10^{6}	32	1.20×10^{-3}	1.13×10^{14}
3	2.41×10^{-2}	3.07×10^{-8}	13	2.73×10^{-2}	8.38×10^{-1}	23	3.32×10^{-2}	2.29×10^{7}	33	8.18×10^{-3}	6.24×10^{14}
4	2.68×10^{-2}	1.70×10^{-7}	14	3.15×10^{-2}	4.64×10^{0}	24	3.20×10^{-2}	1.27×10^{8}	34	8.18×10^{-8}	3.46×10^{15}
5	3.26×10^{-2}	9.43×10^{-7}	15	2.11×10^{-2}	2.57×10	25	2.66×10^{-2}	7.02×10^{8}	35	3.60×10^{-5}	1.91×10^{16}
6	3.86×10^{-2}	5.22×10^{-6}	16	2.05×10^{-2}	1.43×10^{2}	26	1.51×10^{-2}	3.89×10^{9}	36	5.97×10^{-6}	1.06×10^{17}
7	2.58×10^{-2}	2.89×10^{-5}	17	4.37×10^{-2}	7.90×10^{2}	27	2.56×10^{-2}	2.15×10^{10}	37	1.44×10^{-8}	5.88×10^{17}
8	3.68×10^{-2}	1.60×10^{-4}	18	4.63×10^{-2}	4.38×10^{3}	28	2.83×10^{-2}	1.19×10^{11}	38	3.33×10^{-6}	3.26×10^{18}
9	2.55×10^{-2}	8.89×10^{-4}	19	3.79×10^{-5}	2.42×10^{4}	29	1.21×10^{-2}	6.61×10^{11}	39	6.18×10^{-9}	1.80×10^{19}
10	2.16×10^{-2}	4.92×10^{-3}	20	2.59×10^{-2}	1.34×10^{5}	30	1.13×10^{-2}	3.67×10^{12}	40	1.82×10^{-4}	1.00×10^{20}

The effect on the change in the material shear modulus decreases with increasing relaxation time. The total impact on the change in shear modulus does not exceed 2% with a relaxation time of $\tau_i \geq 10^{10}$ s.

3.2.2. Anand Model

The parameters of the Anand elastic-viscoplastic model were also determined. The dependence of the yield strength initial value on temperature is one of the key factors. The stress level for exiting the elasticity theory can be estimated based on the following parameter (Figure 11).

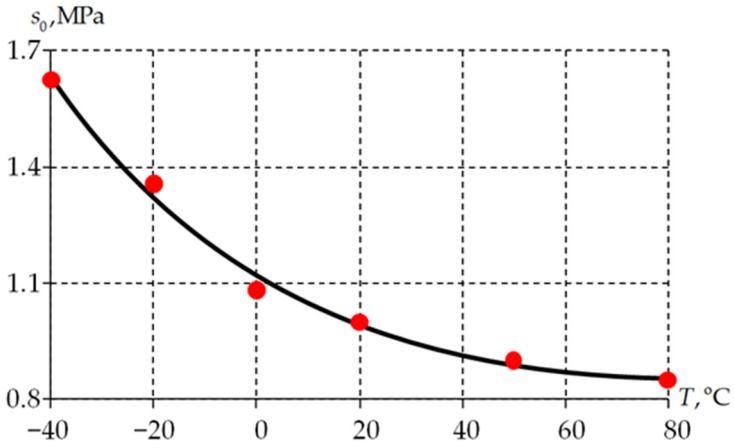


Figure 11. Yield strength initial value dependence on temperature: dots is averaged data; solid line is relation (28).

The yield strength initial value depends on temperature non-linearly. The parameter value decreases with a damping effect as the temperature increases. This may indicate that the yield strength initial value will not be lower than 0.8 MPa with increasing temperature. A rapid increase in yield strength is observed with decreasing temperature. This indicates that the material is close to its glass transition/softening temperature. However, it does not fall within the range being considered. Further experiments will be required to determine the glass transition/softening temperature in future studies. This will cause additional difficulties in generating sub-zero temperatures of less than −40 °C in experiments using liquid nitrogen.

The activation energy temperature dependence is shown in Figure 12.

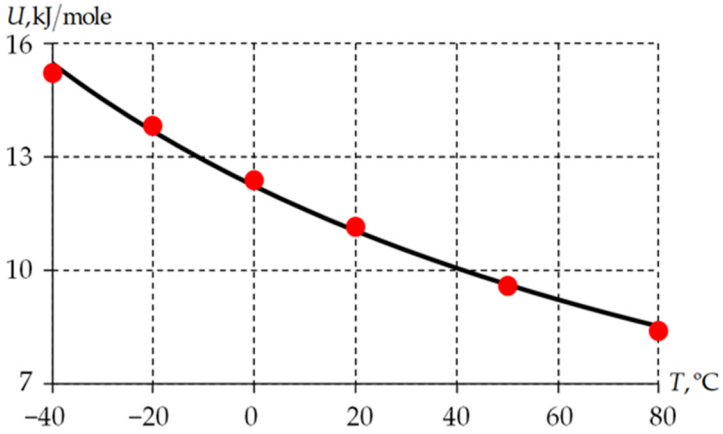


Figure 12. Activation energy dependence on temperature: dots is averaged data; solid line is co-relation (27).

Activation energy dependence on temperature is close to linear. Its parameter corresponds to the range of values of polyvinylchloride, which relates to amorphous materials.

Figure 13 demonstrates the temperature dependence of the strain rate sensitivity factor.

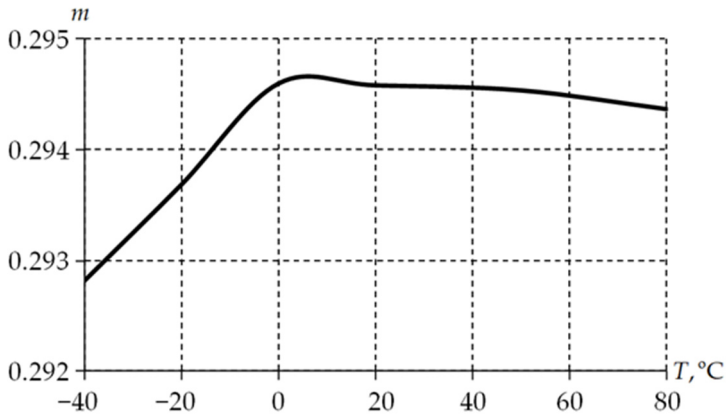


Figure 13. Temperature dependence of the strain rate sensitivity factor.

The strain rate sensitivity factor has a slight variation in values within the temperature range less than 0.01%. It can be considered as constant if necessary. This will entail an additional minor error when simulating the material behavior of actual structures and systems.

The extended Anand model includes the following parameters: $n = 4.53 \times 10^{-3}$; $\xi = 5.01 \times 10^{-5}$; $h_0 = 1.39 \times 10^5$; $\hat{s} = 6.83 \times 10^2$; $a = 6.303$. Constants for describing the temperature dependences of activation energy (27), yield strength (28), and the strain rate sensitivity factor (29) are presented in Table 4.

Table 4. Parameters of relations (27)–(29) of the modified Anand model.

i	U_i	s_{0i}	m_i
1	1.02×10	2.12×10^{-8}	1.02×10^{-1}
2	-4.343	6.39×10^{-3}	7.10×10^{-1}
3	6.83×10	2.05×10^3	-4.27
4	-9.96×10^{-1}	6.01×10^8	7.1×10^{-1}
5	6.46×10^{-1}	-1.36×10^3	-4.27

3.3. Numerical Simulation of the Stress–Strain State of an L-100 Spherical Bridge Bearing with Various Antifriction Layer Material Models

The analysis of the material behavior of the L-100 bridge bearing in an axisymmetric formulation for multi-cycle loading was conducted in the present study. This was performed as part of testing and evaluating thermomechanical models of UHMWPE, which was used as an antifriction layer. The multi-cycle loading effect on the deformation behavior of the material was considered for the constant temperature field. The behavior of the antifriction layer structure and material in the first approximation was considered for three temperatures −40 °C, +20 °C, and +80 °C.

The dependence of the bridge bearing settlement on the number of loading cycles is illustrated in Figure 14.

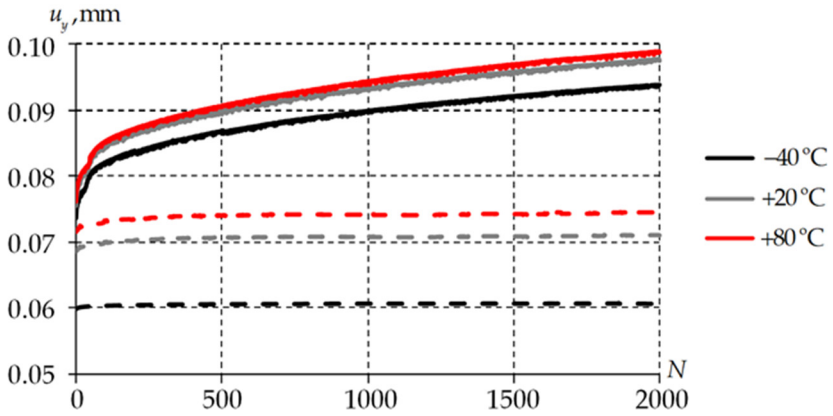


Figure 14. Bridge bearing settlement dependence on the number of loading cycles: solid line is elastic-viscoplastic model; dashed line is viscoelastic model.

The distribution pattern of the vertical displacement of the bridge bearing (the settlement) is nonlinear. Fluctuations of the parameter are associated with the solution of the contact problems and the redistribution of the contact statuses in the course of the iterative solution procedure. The settlement reaches an asymptote with an increase in the number of loading cycles. The maximum level of the bridge bearing vertical displacement with an elastic-viscoplastic model of the material is larger than with a viscoelastic model. This is due to taking into account the plastic deformation of the material, which is observed in this class of materials [64]. The discrepancy between the results decreases at elevated temperatures. The obtained level of maximum vertical displacement of the bearing is consistent with data obtained from static and cyclic laboratory and field tests [65,66].

The dependence of the maximum normal displacements of the relative free edge of the antifriction layer S_{K_3} on the number of loading cycles is illustrated in Figure 15.

The dependence of the maximum displacement level of the end face of the antifriction layer S_{K_3} on the number of loading cycles is nonlinear. Fluctuations of the parameter are associated with changes in the distribution pattern of the contact statuses on the interface surfaces. The maximum normal displacements of the elastic-viscoplastic model are on average 70% higher. The viscoelastic model significantly underestimates the level of the relatively free edge of the antifriction layer.

The elastic-viscoplastic model makes it possible to estimate non-reversible deformations of the antifriction layer. This is its significant advantage over the viscoelastic model. The most dangerous area for the occurrence of such deformations is a stress concentrator in the form of a metal shoulder of the bottom steel plate, in contact with the antifriction layer. The dependence of the maximum plastic deformation values of the antifriction layer on the number of loading cycles is shown in Figure 16.

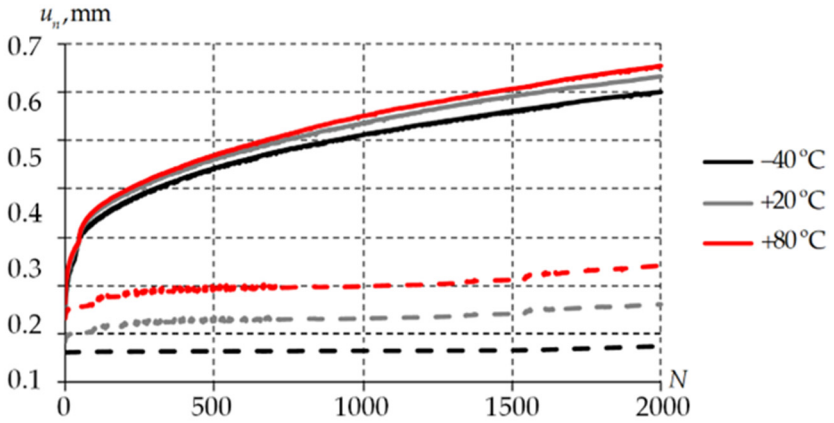


Figure 15. Dependence of the maximum displacement level of the end face of the antifriction layer S_{K_3} on the number of loading cycles: solid line is elastic-viscoplastic model; dashed line is viscoelastic model.

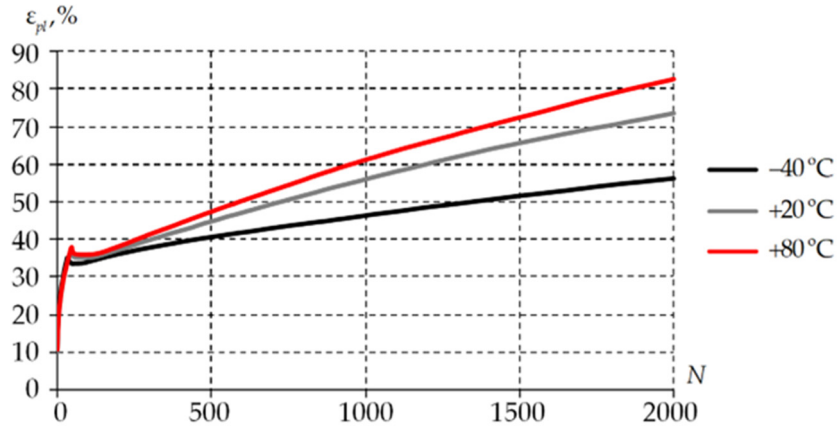


Figure 16. Dependence of the maximum plastic deformation values of the antifriction layer on the number of loading cycles: solid line is elastic-viscoplastic model; dashed line is viscoelastic model.

The growth of plastic deformations results in an increase in the other parameters of the stress–strain state of the structure. Localization of plastic deformations indicates a risky area of the structure: the metal shoulder of the bottom steel plate. When evaluating the geometry of this part of the structure, the operability of the structure should also be assessed in further studies. The level of plastic deformations in the bulk volume of the sliding layer material is insignificant, less than 1% (Figure 17).

The level of plastic deformations does not exceed 1% in the central part of the layer. The level of plastic deformations near the end face of the layer after 2000 loading cycles is about 9% (without taking into account the stress concentrator). Without taking into account plastic deformations of the material, it is possible to obtain overestimated stress values in the polymer antifriction structure. This is confirmed by the current results (Figure 18).

In the viscoelastic model, the equivalent stress strongly increases with increasing the number of loading cycles. However, in the elastic-viscoplastic model of the antifriction layer material, the equivalent stress value significantly decreases with an increase in the number of loading cycles. This indicates a softening of the material during the deformation process. These effects are caused by the presence of a stress/strain concentrator.

The pattern of the stress distribution over the volume of the antifriction layer and maximum values localization zone are consistent with the data obtained by Deng et al. [67]. The PTFE antifriction layer responds to the temperature change in a different way [67]: increasing temperature results in a decrease in the level of the stress–strain state parameters.

This may be due to the fact that the glass transition/softening temperature of the material falls within the considered temperature range [−10; +20] °C.

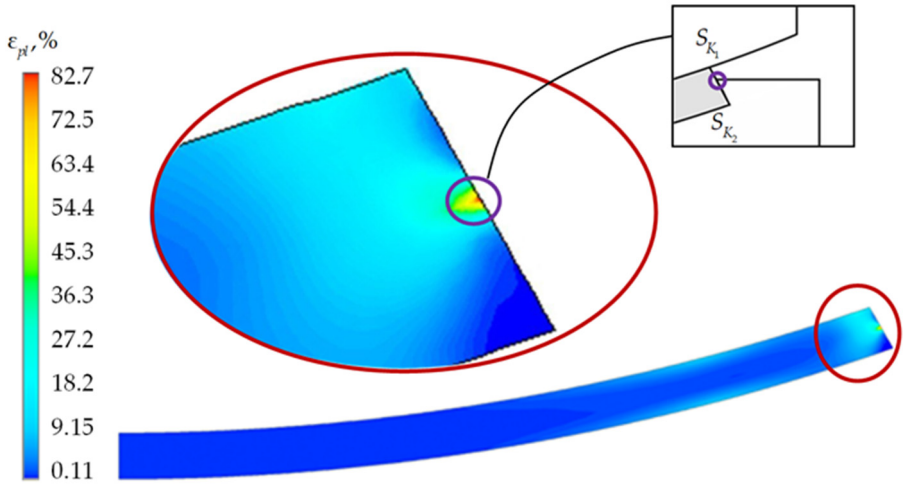


Figure 17. Plastic deformations of the antifriction layer after 2000 loading cycles: red oval is the area near the layer end face with a stress concentrator; violet-colored oval is the area of the maximum plastic deformation level (stress concentrator); black rectangular area is the simplified diagram of the bridge bearing near the end face of the layer.

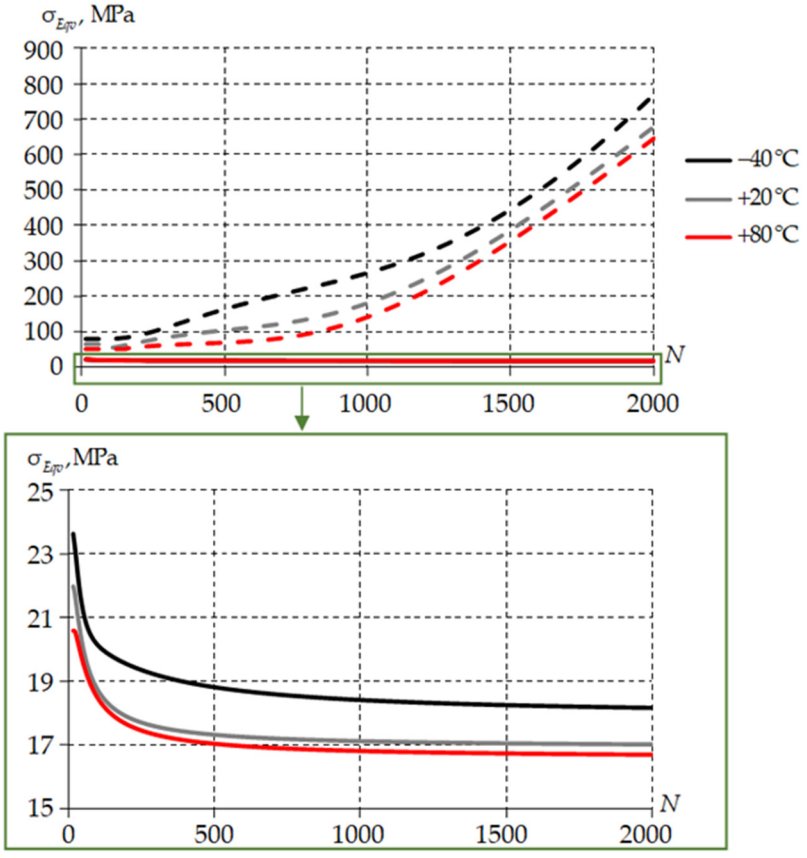


Figure 18. Dependence of the maximum plastic deformation values of the antifriction layer on the number of loading cycles: solid line is elastic-viscoplastic model; dashed line is viscoelastic model; the green frame is approximated by an elastic-viscoplastic model.

Using the material behavior models in the framework of the viscoelasticity theory leads to significant underestimation of the deformation level parameters and overestimation

of the stress state parameters. The viscoelastic material behavior model of the antifriction layer has a large number of limitations when analyzing the behavior of real structures.

4. Discussion

4.1. Limitation Statement

For the current study, the following limitations were set:

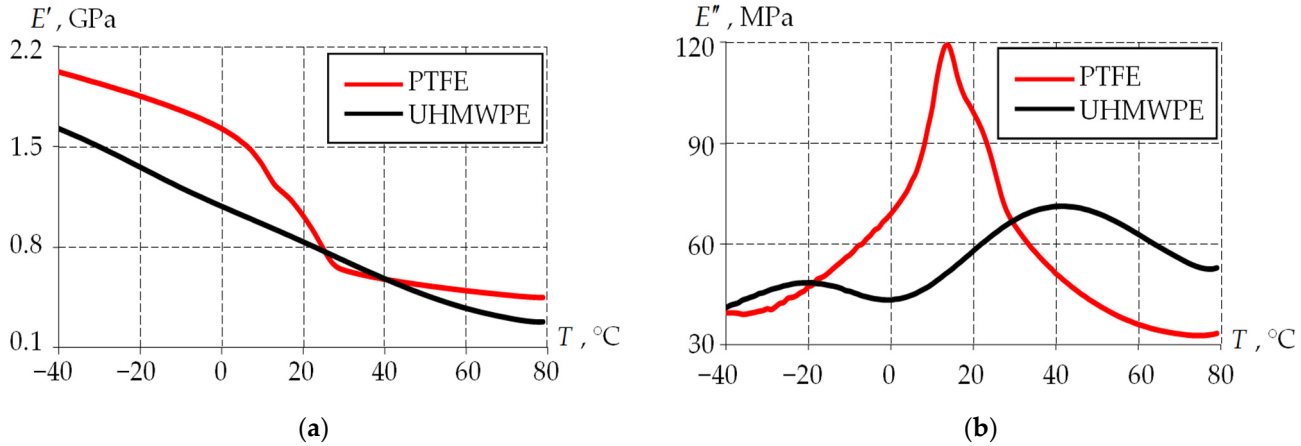
- The temperature range from −40 °C to +80 °C was considered. However, in the bridgeworks, temperatures may occur that fall outside the range under consideration [68,69].
- There is no experimental study of the stress concentrator and its geometry effect on the destruction of the polymer sliding layer.
- No studies of material creep and relaxation have been conducted, but this is important for forming a material behavior model with minimal deviation from reality [70–73].
- Deformation of the structure is considered in an axisymmetric formulation, which does not allow taking into account cavities for lubricant in the antifriction layer in the form of spherical indents.
- Oscillations of the bridgework are not considered when modeling multi-cycle loading during train movement [74–77].

4.2. On the Possibility of Replacing the "Plastic King" with Modern Polymers and Composites

PTFE has been used as the antifriction layer material for bridge bearings and pivot mechanisms for decades since the beginning of the design of steel balance beams [2,78]. New and modified bridge bearing structures are also designed with an antifriction layer made of PTFE [67,79]. However, cases of bearing failure due to plasticity or creeping of the antifriction sliding layer during loading from the bridge span are noted [80]. The stress–strain state of a structure with a PTFE antifriction layer is significantly inferior to analogs with antifriction layers made of modern antifriction materials. The level of the normal displacements of the end face of the layer made of this material is 25–30% higher than in structures using composites based on it, and 85–90% higher when modern antifriction materials are used [78]. A permanent increase in the tonnage of bridgeworks has further revealed the shortcomings of PTFE antifriction layers [2]. PTFE limitations and the need to modify it by introducing various additives or replacing it with modern polymers and composites are comprehensively discussed by the scientific community [81–83]. UHMWPE is considered as an alternative to PTFE, including for the purposes of friction units [2,20,84,85], because it can better retain its shape and structural integrity, is more resistant to erosion, has improved shear strength, etc.

World leaders in the design and manufacture of bridge bearings, MAGEBA SA (Bulach, Switzerland) [86] and MAURER SE (Munich, Germany) [87], are also abandoning the use of PTFE as a sliding layer. The highly durable and wear-resistant material based on modified high-molecular-weight polyethylene ROBO®SLIDE is used by MAGEBA SA (Bulach, Switzerland) for antifriction layers [86]. Modified UHMWPE with various additives MAURER Sliding Material (MSM®) is a patented material of the bridge bearing sliding layers manufactured by MAURER SE (Munich, Germany) [87–89]. However, Adamov et al. note the lack of data on the properties of the materials considering operating temperatures and nonlinear effects in the public domain [5]. This is a limiting factor for the implementation of UHMWPE, its compositions and modifications, as well as the other alternatives in friction units. The current material provides data on the thermomechanical and physicomechanical properties of one of the UHMWPE variants. The data can form the basis for digital analysis of the possibility of using UHMWPE as coatings and antifriction layers for highly loaded friction units.

Currently, UHMWPE can be compared with PTFE within the DMA (Figure 19). The experiments have been fully conducted and processed.



(**a**) (**b**)

Figure 19. Comparison of the experimentally determined thermomechanical properties of PTFE and UHMWPE: (**a**) is storage modulus; (**b**) is loss modulus.

PTFE glass transition/softening temperature falls into the temperature range being considered. This is indicated by a decrease in the storage modulus and a peak of the loss modulus observed in the temperature range from 0 to 20 °C. The glass transition/softening temperature is 8–14 °C, depending on different definition theories. PTFE is less resistant to temperature changes. The material changes from a glassy state to a rubbery state in the operating temperature range of the bridge bearing. In the range of +30 °C, UHMWPE exhibits a higher elastic response than PTFE. The viscosity of UHMWPE is higher than that of PTFE in two temperature ranges, from −40 °C to +20 °C, and from +30 °C to +80 °C.

In addition, numerical simulation of PTFE viscoelastic behavior was performed; free compression tests and CTE determination of the material must be carried out. They are planned for the end of 2025—beginning of 2026. Comparative analysis of the materials will be carried out as part of the study development after the formation of the modified Anand model for PTFE based on an identical set of experimental data. The PTFE thermal expansion coefficient will have a more complex dependence on temperature. This can be assumed since its glass transition/softening temperature falls into the temperature range under consideration. This fact will have an impact on the experiment. This would require increasing the number of control points within the experiment, as implemented by Shardakov et al. [90].

Whether it can be said that the “plastic king” [91] (PTFE) has gradually begun to lose its crown, time will tell. However, the first steps toward changing the favorite in the field of antifriction polymer materials have already been made. The current work also confirms that there are materials with a more stable structure over the operating temperature range of bridgeworks. The presented materials can be widely used not only in the design of bridgeworks, but also in other branches of science and technology [1,92–94].

5. Conclusions

An experimental study of UHMWPE aimed at determining the thermomechanical, thermophysical, and physical-mechanical properties in a wide temperature range was carried out as a part of the current work. Phenomenological relationships of viscoelasticity and elastic-viscoplasticity were created to describe the behavior of the material. Maxwell and Anand models were selected to evaluate the feasibility of their application to describe the thermomechanics of UHMWPE. The temperature dependence of a number of parameters had to be introduced into the Anand model to modify it to minimize the discrepancy

between the digital model and the test data. Vectors of unknown parameters of models for CAD systems (ANSYS, ABAQUS, etc.) were formed and identified based on the experimental data.

Material behavior models were tested within the framework of the spherical bridge bearing stress–strain state analysis under multi-cycle loading conditions. It was established that the viscoelastic model made it possible to obtain underestimated deformation characteristics and overestimated stress state parameters. Taking into account the plastic deformation of UHMWPE is necessary for forming a high-quality digital analog of both the material and the structures and systems in which it is used.

Expansion of the phenomenological relations of the Anand model by the introduction of the temperature dependence of a number of parameters is an important part of the current work. It has been established that the viscoelastic model in the form of a generalized Maxwell body is insufficient for describing material behavior under multi-cycle loading conditions. The elastic-viscoplastic model demonstrated its efficiency and can be used to describe a number of materials, such as polymers, composites, grease lubricants, etc.

Modeling the behavior of materials using the well-established nonlinear viscoelastic model parallel rheological framework PRF [95] and recently proposed models [96,97] can be considered as a development of the work.

Author Contributions: Conceptualization, A.A.K., Y.O.N. and A.P.B.; methodology, A.A.K.; software, A.A.K., A.P.B., Y.O.N. and A.R.M.; validation, A.A.K. and Y.O.N.; writing—original draft preparation, A.P.B. and Y.O.N.; writing—review and editing, A.A.K. and A.R.M.; visualization, A.A.K., Y.O.N. and A.P.B.; funding acquisition, A.P.B. All authors have read and agreed to the published version of the manuscript.

Funding: The study was supported by the Russian Science Foundation grant No. 25-29-00638, https://rscf.ru/project/25-29-00638/ (accessed on 28 October 2025).

Institutional Review Board Statement: Not applicable.

Informed Consent Statement: Not applicable.

Data Availability Statement: The original contributions presented in this study are included in the article. Further inquiries can be directed to the corresponding author.

Conflicts of Interest: The authors declare no conflicts of interest.

References

1. Cholewa, K.; Kurtyka, P.; Janiczak, K.; Kapis, A.; Szuber-Dynia, A.; Janecki, M.; Walke, W.; Wilk, K.; Gawlikowski, M. Mechanical and Hemocompatibility Assessment of Selected Technologies for Prosthesis Connection with the Outflow Cannula Graft of the RH PED Pediatric Pulsatile Pump for Heart Support. *J. Clin. Med.* **2025**, *14*, 4621. [CrossRef] [PubMed]
2. Li, Y.; Guo, W.; Huang, X.; Chen, Z.; Gao, Y. Friction Characteristics and Lubrication Properties of Spherical Hinge Structure of Swivel Bridge. *Lubricants* **2024**, *12*, 130. [CrossRef]
3. Liu, Q.; Xiong, J.; Lin, W.; Liu, J.; Wan, Y.; Guo, C.F.; Wang, Q.; Liu, Z. Porous polymers: Structure, fabrication and application. *Mater. Horiz.* **2025**, *12*, 2436–2466. [CrossRef]
4. Satchanska, G.; Davidova, S.; Petrov, P.D. Natural and synthetic polymers for biomedical and environmental applications. *Polymers* **2024**, *16*, 1159. [CrossRef] [PubMed]
5. Adamov, A.A.; Keller, I.E.; Ostrer, S.G.; Seletkov, D.V. Evaluation of the Performance of Antifriction PTFE Composites at a Pressure Over 60 MPA. I. Comparison of Their Hardness and Deformation Properties Under Free and Constrained Compression. *Mech. Compos. Mater.* **2022**, *58*, 673–688. [CrossRef]
6. Adamov, A.A.; Kamenskih, A.A.; Pankova, A.P. Numerical analysis of the spherical bearing geometric configuration with antifriction layer made of different materials. *PNRPU Mech. Bull.* **2020**, *4*, 15–26. [CrossRef]
7. Xiang, S.; Long, X.; Zhang, Q.; Ma, P.; Yang, X.; Xu, H.; Lu, P.; Su, P.; Yang, W.; He, Y. Enhancing Lubrication Performance of Calcium Sulfonate Complex Grease Dispersed with Two-Dimensional MoS2 Nanosheets. *Lubricants* **2023**, *11*, 336. [CrossRef]
8. Srivastav, R.S.; More, A.P. A Comprehensive Review of Self-Healing Polymers: Mechanisms, Types, and Industry Implications. *Polym. Adv. Technol.* **2025**, *36*, 70092. [CrossRef]

9. Sabet, M. Revolutionizing structures: The rise of high-performance composite and nanocomposite polymers. *Polym. Bull.* **2025**, *82*, 4257–4306. [CrossRef]
10. Shepelenko, I.; Nemyrovskyi, Y.; Stepchyn, Y.; Mahopets, S.; Melnyk, O. Creation of a Combined Technology for Processing Parts Based on the Application of an Antifriction Coating and Deforming Broaching. *Lect. Notes Mech. Eng.* **2024**, *327*, 209–218. [CrossRef]
11. Petrova, P.N.; Markova, M.A.; Chernykh, V.D. Investigation of Properties of Polytetrafluoroethylene-Based Composites and Carbon Fibers Depending on the Production Technology. *Inorg. Mater. Appl. Res.* **2024**, *15*, 17–25. [CrossRef]
12. Gupta, S.; Iyer, R.S.; Kumar, S. *Digital Twins*; Springer: Cham, Switzerland, 2025. [CrossRef]
13. Smetannikov, O.Y.; Il'inykh, G.V.; Faskhutdinova, Y.B. A model of the thermomechanical behavior of shape-memory photopolymers under thermorelaxa-tion transition conditions. *Tomsk. State Univ. J. Math. Mech.* **2025**, *97*, 168–183.
14. Vindokurov, I.; Pirogova, Y.; Tashkinov, M.; Silberschmidt, V.V. Compression of additively manufactured PLA for biomedical applications: Effects of test conditions on properties of solid samples. *Polym. Test.* **2024**, *130*, 108320. [CrossRef]
15. Jinaga, U.K.; Zulueta, K.; Burgoa, A.; Cobian, L.; Freitas, U.; Lackner, M.; Major, Z.; Noels, L. A consistent finite-strain thermomechanical quasi-nonlinear-viscoelastic viscoplastic constitutive model for thermoplastic polymers. *Int. J. Solids Struct.* **2025**, *321*, 13517. [CrossRef]
16. Kamal, A.; Mosleh, A.O.; Gaafer, A.; Youness, R.A.; Taha, M.A. High-performance PTFE composites from industrial scrap with enhanced strength and wear resistance. *Sci. Rep.* **2025**, *15*, 28445. [CrossRef]
17. Yu, S.; Zhu, C.; Wu, H.; Yao, L.; Mahapatra, M.; Xu, Y. Graphite-Enhanced PTFE/PEEK composite coating for improved friction and wear resistance. *Appl. Surf. Sci.* **2025**, *700*, 163214. [CrossRef]
18. Yuan, L.; Zheng, X.; Zhu, W.; Wang, B.; Chen, Y.; Xing, Y. Study on the Electrical Insulation Properties of Modified PTFE at High Temperatures. *Polymers* **2024**, *16*, 316. [CrossRef]
19. Elaboudi, I.; Mdarhri, A.; Brosseau, C.; Nourdine, A.; Rzaizi, M.; Servant, L. Comparing the sorption kinetics of polytetrafluoroethylene processed either by extrusion or spark plasma sintering. *Polymer* **2020**, *190*, 122192. [CrossRef]
20. Park, J.-H.; Lee, J.-W. Friction Behavior of Ceramic Materials for the Development of Bridge-Bearing Friction Materials. *Appl. Sci.* **2025**, *15*, 152. [CrossRef]
21. Savin, L.; Pinteala, T.; Mihai, D.N.; Mihailescu, D.; Miu, S.S.; Sirbu, M.T.; Veliceasa, B.; Popescu, D.C.; Sirbu, P.D.; Forna, N. Updates on Biomaterials Used in Total Hip Arthroplasty (THA). *Polymers* **2023**, *15*, 3278. [CrossRef]
22. Kalácska, Á.; Parmentier, V.; De Baets, P.; Kalácska, G. Wear investigation of PTFE. PEEK and UHMWPE-based reciprocating shaft seal materials with lunar/Martian regolith stimulants. *Wear* **2025**, *571*, 205791. [CrossRef]
23. Singh, D.K.; Verma, R.K. Contemporary Development on the Performance and Functionalization of Ultra High Molecular Weight Polyethylene (UHMWPE) for Biomedical Implants. *Nano Life* **2021**, *11*, 2130009. [CrossRef]
24. Abdul Samad, M. Recent Advances in UHMWPE/UHMWPE Nanocomposite/UHMWPE Hybrid Nanocomposite Polymer Coatings for Tribological Applications: A Comprehensive Review. *Polymers* **2021**, *13*, 608. [CrossRef]
25. Assma, S. Ultra-High-Molecular-Weight-Polyethylene (UHMWPE) as Desired Polymer Material for Biomedical. *Khalij-Libya J. Dent. Med. Res.* **2021**, *6*, 11–16. [CrossRef]
26. Yang, C.; Zhang, J.; Yue, H.; Kang, X. The Low Friction Coefficient and High Wear Resistance UHMWPE: The Effect of Pores on Properties of Artificial Joint Materials. *Lubricants* **2025**, *13*, 31. [CrossRef]
27. Bogdanova, A.P.; Kamenskikh, A.A.; Nosov, Y.O. The Geometric Configuration of Lubricant Recesses of the Polymer Sliding Layer of the Bearing. *Designs* **2023**, *7*, 144. [CrossRef]
28. Kamenskikh, A.A.; Nosov, Y.O.; Bogdanova, A.P. The Study Influence Analysis of the Mathematical Model Choice for Describing Polymer Behavior. *Polymers* **2023**, *15*, 3630. [CrossRef]
29. Münstedt, H. Rheological measurements and structural analysis of polymeric materials. *Polymers* **2021**, *13*, 1123. [CrossRef] [PubMed]
30. Gan, Z.; Liu, J.; Xu, Z.; Jia, S.; Dong, X.-H. Precision polymers: Advances in synthesis, structural engineering, and functional optimization. *Prog. Polym. Sci.* **2025**, *170*, 102030. [CrossRef]
31. Barnes, A.H. *A Handbook of Elementary Rheology*; University of Wales Institute of Non-Newtonian Fluid Mechanics: Aberystwyth, UK, 2000.
32. Nosov, Y.O.; Kamenskikh, A.A. Experimental Study of the Rheology of Grease by the Example of CIATIM-221 and Identification of Its Behavior Model. *Lubricants* **2023**, *11*, 295. [CrossRef]
33. Vidakis, N.; Petousis, M.; Mountakis, N.; David, C.N.; Sagris, D.; Das, S.C. Thermomechanical response of thermoplastic polyurethane used in MEX additive manufacturing over repetitive mechanical recycling courses. *Polym. Degrad. Stab.* **2023**, *207*, 110232. [CrossRef]
34. Ardıç, S.; Kunt, G.; Gürgen, S.; Pat, S. UHMWPE Based Composites with CNT Fillers: Surface, Mechanical and Electrical Aspects. *Mater. Res. Bull.* **2025**, *192*, 113634. [CrossRef]

35. Rahman, M.; Biswas, A.S.; Hoque, K.N. Recent development on micro-texturing of UHMWPE surfaces for orthopedic bearings: A review. *Biotribology* **2022**, *31*, 100216. [CrossRef]
36. Leksycki, K.; Feldshtein, E.; Maruda, R.W.; Khanna, N.; Królczyk, G.M.; Pruncu, C.I. An insight into the effect surface morphology, processing, and lubricating conditions on tribological properties of Ti6Al4V and UHMWPE pairs. *Tribol. Int.* **2022**, *170*, 107504. [CrossRef]
37. Beiras, R.; Verdejo, E.; Campoy-López, P.; Vidal-Liñán, L. Aquatic toxicity of chemically defined microplastics can be explained by functional additives. *J. Hazard. Mater.* **2021**, *406*, 124338. [CrossRef]
38. Maraveas, C.; Kyrtopoulos, I.V.; Arvanitis, K.G.; Bartzanas, T. The aging of polymers under electromagnetic radiation. *Polymers* **2024**, *16*, 689. [CrossRef]
39. Nosov, Y.O.; Kamenskikh, A.A. Influence Analysis of Lubricant Recesses on the Working Capacity of the Bridge Span Spherical Bearing. *Lubricants* **2022**, *10*, 283. [CrossRef]
40. Wang, J.; Sun, J.; Sun, S.; Zhang, H.; Wang, Q.; Yang, J.; Mei, Y. Numerical simulation of electromagnetically induced transparency in composite metamaterial. *Phys. Scr.* **2025**, *100*, 025512. [CrossRef]
41. Sivtsev, P.V. Simplified numerical homogenization method for the plasticity problem with isotropic hardening. *Lobachevskii J. Math.* **2023**, *44*, 4157–4169. [CrossRef]
42. Stankiewicz, A. On applicability of the relaxation spectrum of fractional maxwell model to description of unimodal relaxation spectra of polymers. *Polymers* **2023**, *15*, 3552. [CrossRef]
43. Dinzart, F.; Torres-Costa, L.M.; Sabar, H. New micromechanical model in time domain for linear viscoelastic composites with ellipsoidal reinforcements. *Acta Mech.* **2022**, *233*, 2009–2029. [CrossRef]
44. Nosov, Y.O.; Kamenskikh, A.A.; Bogdanova, A.P. Description of the Lubricant Behavior Based on the Theory of Elasto-Viscoplastic. *Materials* **2025**, *18*, 1360. [CrossRef]
45. Hu, Q.; Pei, Q.; Li, P. Reducing the Friction Coefficient of Heavy-Load Spherical Bearings in Bridges Using Surface Texturing—A Numerical Study. *Lubricants* **2025**, *13*, 180. [CrossRef]
46. Yang, Y.; Zhang, Y.; Ju, J. Study on the mechanical properties of a type of spherical bearing. *J. Theor. Appl. Mech.* **2021**, *59*, 539–550. [CrossRef]
47. Eggert, H.; Kauschke, W. *Structural Bearings*; Ernst & Sohn: Berlin, Germany, 2002.
48. Nowacki, W.; Koźniewska, I.; Brandt, A.M. *Théorie du Fluage*; Eyrolles: Paris, France, 1965.
49. Smetannikov, O.Y.; Sakhabutdinova, L.; Ilyinykh, G. ANSYS Simulation of the Thermomechanical Behavior of a Large-Sized Composite Mandrel with Consideration of Viscoelasticity. *Aerospace* **2022**, *9*, 117. [CrossRef]
50. Adamov, A.A.; Keller, I.E.; Petukhov, D.S.; Kuzminykh, V.S.; Patrakov, I.M.; Grakovich, P.N.; Shilko, I.S. Evaluation of the Performance of PTFE-Composites as Antifriction Layers in Supporting Parts with a Spherical Segment. *J. Frict. Wear* **2023**, *44*, 127–134. [CrossRef]
51. Wang, D.; de Boer, G.; Neville, A.; Ghanbarzadeh, A. A Review on Modelling of Viscoelastic Contact Problems. *Lubricants* **2022**, *10*, 358. [CrossRef]
52. Itou, H.; Kovtunenko, V.A.; Nakamura, G. Forward and inverse problems for creep models in viscoelasticity. *Philos. Trans. A* **2024**, *382*, 20230295. [CrossRef] [PubMed]
53. Lin, C.Y. Rethinking and researching the physical meaning of the standard linear solid model in viscoelasticity. *Mech. Adv. Mater. Struct.* **2023**, *31*, 2370–2385. [CrossRef]
54. Dundar, M.A.; Dhaliwal, G.S.; Nuraliyev, M.; Ayorinde, E.O. Numerical prediction of mechanical behavior of acrylonitrile-butadiene-styrene under three-point bending and impact loadings by Anand–Gurtin material model. *Proc. Inst. Mech. Eng. Part C J. Mech. Eng. Sci.* **2022**, *236*, 11024–11040. [CrossRef]
55. Li, K.; Deng, H.; Xu, W.; Liu, Y. Modelling of fracture-involved large strain behaviors of amorphous glassy polymers via a unified physically-based constitutive model coupled with phase field method. *Eng. Fract. Mech.* **2024**, *311*, 110546. [CrossRef]
56. Sun, H.; Yan, Z.; Wu, S.; Liu, Z.; Jiang, Y. A Study on the Cavitation Effect of Elastic Material with Textured Surfaces under Fluid Lubrication Conditions. *Machines* **2024**, *12*, 267. [CrossRef]
57. Fusek, M.; Paška, Z.; Rojíček, J.; Fojtík, F. Parameters Identification of the Anand Material Model for 3D Printed Structures. *Materials* **2021**, *14*, 587. [CrossRef]
58. Kamenskikh, A.; Bogdanova, A.; Nosov, Y. Nonlinear Behavior of Greases: Experiment, Identification, Model. *Lubr. Sci. Chall. Emerg. Technol.* **2025**, *2025*, 1011633. [CrossRef]
59. Darby, S.P.; Landrum, D.B.; Coleman, H.W. Assessment of Uncertainty in the Determination of Activation Energy for Polymeric Materials. *J. Thermophys. Heat Transf.* **1998**, *12*, 520–527. [CrossRef]
60. Yang, M.; Li, W.; Dong, P.; Ma, Y.; He, Y.; Zhao, Z.; Chen, L. Temperature and strain rate sensitivity of yield strength of amorphous polymers: Characterization and modeling. *Polymer* **2022**, *251*, 124936. [CrossRef]
61. Sanditov, D.S.; Mashanov, A.A.; Razumovskaya, I.V. On the Temperature Dependence of the Glass Transition Activation Energy. *Polym. Sci. Ser. A* **2020**, *62*, 588–596. [CrossRef]

62. Kamenskikh, A.A.; Bogdanova, A.P.; Nosov, Y.O.; Kuznetsova, Y.S. Influence of the Pattern of Coupling of Elements and Antifriction Interlayer Thickness of a Spherical Bearing on Structural Behavior. *Designs* **2025**, *9*, 117. [CrossRef]
63. Kamenskih, A.A.; Trufanov, N.A. Regularities of interactions between elements of a spherical contact unit with an antifriction polymeric interlayer. *J. Frict. Wear* **2015**, *36*, 170–176. [CrossRef]
64. Petukhov, D.S.; Adamov, A.A.; Keller, I.E. Selection and Identification of a Model of Elasto-Viscoplasticity of the Filled Fluorocomposite according to Free and Constrained Compression Tests. *Adv. Eng. Res.* **2022**, *22*, 180–192. [CrossRef]
65. Chen, S.; Zhou, Y.; Xie, K.; Zhang, P.; Li, C. Dynamic Adaptability of Spherical Bearings in Small-Span Bridges for Heavy-Haul Railways. *Buildings* **2025**, *15*, 619. [CrossRef]
66. Yan, L.; Gou, X.Y.; Zhang, X.; Jiang, Y.; Ran, X.W.; Zhang, P. Experimental and Numerical Investigations on the Spherical Steel Bearing Capacity of New Anti-Separation Design. *KSCE J. Civ. Eng.* **2024**, *28*, 889–903. [CrossRef]
67. Deng, N.; He, M.; Gu, N.; Liang, H. Design and Performance Research of a New Type of Spherical Force-Measuring Bearing of Bridges Based on Button Type Microsensor. *KSCE J. Civ. Eng.* **2024**, *28*, 5066–5076. [CrossRef]
68. Yang, D.-H.; Guan, Z.-X.; Yi, T.-H.; Li, H.-N.; Liu, H. Structural temperature gradient evaluation based on bridge monitoring data extended by historical meteorological data. *Struct. Health Monit.* **2023**, *23*, 1800–1815. [CrossRef]
69. Li, L.; Chen, B.; Zhou, L.; Xia, Q.; Zhou, Y.; Zhou, X.; Xia, Y. Thermal behaviors of bridges—A literature review. *Adv. Struct. Eng.* **2023**, *26*, 985–1010. [CrossRef]
70. Duan, X.; Yuan, H.; Tang, W.; He, J.; Guan, X. A Phenomenological Primary–Secondary–Tertiary Creep Model for Polymer-Bonded Composite Materials. *Polymers* **2021**, *13*, 2353. [CrossRef]
71. Jiang, Z.; Fang, Z.; Fang, C.; Li, Q.; Wang, Z. Experimental investigation on high-temperature creep behavior of carbon fiber reinforced polymer cable. *Compos. Struct.* **2023**, *291*, 115533. [CrossRef]
72. Zhao, Y.; Xiao, H.; Chen, L.; Chen, P.; Lu, Z.; Tang, C.; Yao, H. Application of the non-linear three-component model for simulating accelerated creep behavior of polymer-alloy geocell sheets. *Geotext. Geomembr.* **2025**, *53*, 70–80. [CrossRef]
73. Chang, Z.; Wang, Y.; Zhang, Z.; Gao, K.; Hou, G.; Shen, J.; Zhang, L.; Liu, J. Creep behavior of polymer nanocomposites: Insights from molecular dynamics simulation. *Polymer* **2021**, *228*, 123895. [CrossRef]
74. Li, Y.; Xiang, H.; Wang, Z.; Zhu, J. A comprehensive review on coupling vibrations of train–bridge systems under external excitations. *Railw. Eng. Sci.* **2022**, *30*, 383–401. [CrossRef]
75. Erduran, E.; Pettersen, F.M.; Gonen, S.; Lau, A. Identification of Vibration Frequencies of Railway Bridges from Train-Mounted Sensors Using Wavelet Transformation. *Sensors* **2023**, *23*, 1191. [CrossRef]
76. Erduran, E.; Gonen, S.; Alkanany, A. Parametric analysis of the dynamic response of railway bridges due to vibrations induced by heavy-haul trains. *Struct. Infrastruct. Eng.* **2022**, *20*, 326–339. [CrossRef]
77. Zhai, Z.; Zhu, S.; Yang, Y.; Luo, J.; Cai, C. Dynamics analysis of train-track-bridge coupled system considering spatial flexibility of high piers and system longitudinal vibrations. *Veh. Syst. Dyn.* **2022**, *61*, 2613–2637. [CrossRef]
78. Adamov, A.A.; Kamenskikh, A.A.; Pankova, A.P.; Strukova, V.I. Comparative analysis of the work of bridge spherical bearing at different antifriction layer locations. *Lubricants* **2022**, *10*, 207. [CrossRef]
79. Liu, X.; Zhao, P.; Chen, Y.; Huang, B.; Wu, Z.; Yang, K.; Weng, Z. Seismic Performance of Long-Span Continuous Rigid-Frame Bridge Equipped with Steel Wire Rope Damper Isolation Bearings. *Buildings* **2025**, *15*, 3249. [CrossRef]
80. Roeder, C.W.; Stanton, J.F.; Campbell, T.I. Rotation of High Load Multirotational Bridge Bearings. *J. Struct. Eng.* **1995**, *121*, 747–756. [CrossRef]
81. Dong, Z.; Tang, H.; Yang, B.; Wang, S.; Li, Y.; Liu, L. Molecular Dynamics Simulation and Experimental Study of the Mechanical and Tribological Properties of GNS-COOH/PEEK/PTFE. *Compos. Polym.* **2024**, *16*, 2572. [CrossRef]
82. Lv, W.; Wang, T.; Wang, Q.; Yap, K.K.; Song, F.; Wang, C. Tribological and Mechanochemical Properties of Nanoparticle-Filled Polytetrafluoroethylene Composites under Different Loads. *Polymers* **2024**, *16*, 894. [CrossRef] [PubMed]
83. Tóth, L.F.; De Baets, P.; Szebényi, G. Thermal, Viscoelastic, Mechanical and Wear Behaviour of Nanoparticle Filled Polytetrafluoroethylene: A Comparison. *Polymers* **2020**, *12*, 1940. [CrossRef] [PubMed]
84. Lian, L.; Haitao, D.; Dan, J.; Jiesong, T.; Shengpeng, Z.; Yinhua, L.; Xiaoshuang, L.; Wen, Z.; Wei, X.; Jian, L. Effect of Contact Pressure on Reciprocating Wear Behavior of PEEK, PTFE, and UHMWPE. *Polym. Korea* **2020**, *44*, 827–834. [CrossRef]
85. Li, R.; Jia, D.; Ma, L.; Yang, T.; Huang, S.; Duan, H.; Cheng, B.; Zhan, S. Study on Cavitation Erosion Mechanism of Ultra-High Molecular Weight Polyethylene (UHMWPE) and Polytetrafluoroethylene (PTFE). *Tribol. Trans.* **2024**, *67*, 1282–1293. [CrossRef]
86. MAGEBA. Available online: https://www.mageba-group.com (accessed on 31 July 2025).
87. MAURER. Available online: https://www.maurer.eu (accessed on 31 July 2025).
88. Huber, P.; Bresler, M.; Paroli, L.; Kruzel, U. Seismic Isolation Protection System for the 1081-Bed Eskisehir City Hospital in Turkey. In Proceedings of the IABSE Symposium Wroclaw 2020—Synergy of Culture and Civil Engineering—History and Challenges, Wrocław, Poland, 7–9 October 2020; pp. 773–780. [CrossRef]
89. Huber, P.; Bresler, M. Seismic Isolation Protection System for the 1081-bed Eskişehir City Hospital in Turkey. *Earthq. Eng. Constr. Saf.* **2019**, *4*, 40–47.

90. Shardakov, I.N.; Trufanov, A.N. Identification of the Temperature Dependence of the Thermal Expansion Coefficient of Polymers. *Polymers* **2021**, *13*, 3035. [CrossRef] [PubMed]
91. Liang, X.; Wu, P.; Lan, L.; Wang, Y.; Ning, Y.; Wang, Y.; Qin, Y. Effect of Polytetrafluoroethylene (PTFE) Content on the Properties of Ni-Cu-P-PTFE Composite Coatings. *Materials* **2023**, *16*, 1966. [CrossRef] [PubMed]
92. Zhuravleva, I.Y.; Dokuchaeva, A.A.; Vaver, A.A.; Kreiker, L.V.; Kuznetsova, E.V.; Grek, R.I. Biopolymer/Suture Polymer Interaction: Is It a Key of Bioprosthetic Calcification? *Polymers* **2025**, *17*, 1576. [CrossRef]
93. Sun, F.; Zhang, X.; Xue, T.; Cheng, P.; Yu, T. The Performance Testing and Analysis of Common New Filter Materials: A Case of Four Filter Materials. *Materials* **2024**, *17*, 2802. [CrossRef]
94. Li, W.; Yao, W.; Zhu, W.; Li, W.; Hong, B.; Wang, X. Mechanical Properties and Constitutive Model of High-Mass-Fraction Pressed Tungsten Powder/Polytetrafluoroethylene-Based Composites. *Polymers* **2025**, *17*, 323. [CrossRef]
95. Hesebeck, O. An Abaqus user subroutine solving convergence problems of nonlinear viscoelastic models with thermorheologically simple temperature dependence. *Int. J. Non-Linear Mech.* **2025**, *172*, 105034. [CrossRef]
96. Katsiropoulos, C.V.; Giannopoulos, G.I.; Pappas, P.; Galiotis, C. Enhancing CFRP damping with graphene nanoplatelets: Experiments versus finite element analysis. *Nanotechnology* **2025**, *36*, 125702. [CrossRef]
97. Kakavas-Papaniaros, P.A.; Giannopoulos, G.I. Nonlinear analysis for propellant solids. *Contin. Mech. Thermodyn.* **2022**, *34*, 1159–1171. [CrossRef]

Disclaimer/Publisher's Note: The statements, opinions and data contained in all publications are solely those of the individual author(s) and contributor(s) and not of MDPI and/or the editor(s). MDPI and/or the editor(s) disclaim responsibility for any injury to people or property resulting from any ideas, methods, instructions or products referred to in the content.